

Article

# Ni@C/PPy Composites Derived from Ni-MOF Materials for Efficient Microwave Absorption

Yu Ma, Yupeng Zou, Lingsai Meng, Lijuan Cai, Shengxiang Xiong, Gang Chen, Chengjun Dong and Hongtao Guan \* 

Yunnan Key Laboratory of Electromagnetic Materials and Devices, National Center for International Research on Photoelectric and Energy Materials, School of Materials and Energy, Yunnan University, Kunming 650091, China; yu1426327038@163.com (Y.M.); 15687852762@163.com (Y.Z.); hello2021mls@163.com (L.M.); 18398914371@163.com (L.C.); 97040404@163.com (S.X.); chengangk@ynu.edu.cn (G.C.); dongcj@ynu.edu.cn (C.D.)

\* Correspondence: htguan06@ynu.edu.cn

**Abstract:** Ni-MOF, as a metal–organic framework, has the advantages of morphological diversity and adjustable composition, which make its derivatives attractive for electromagnetic wave absorption. However, it is challenging for Ni-MOF derivatives to obtain strong absorption at low filling rates. Herein, ternary Ni@C/PPy composites based on Ni-MOF derivatives were synthesized by cooperatively coupling magnetic Ni@C nanoparticles with a conductive polymer PPy matrix through a facile self-assembly method. Among them, Ni@C nanoparticles are formed after Ni-MOF pyrolysis, and PPy serves as the backbone to effectively assemble and support the Ni@C nanoparticles. As a result, the Ni@C/PPy-3 sample exhibited excellent performance with a reflection loss value of  $-50.65$  dB at a filling ratio of 15 wt% and a thickness of 2.5 mm. At the same time, its effective absorption bandwidth reached 6.24 GHz, covering the whole Ku frequency band. The results show that in comparison to pure Ni@C composite, the Ni@C/PPy multi-component composite with a porous structure shows significant advantages in terms of optimizing impedance matching, which can effectively enhance the interface polarization and, thus, greatly improve its electromagnetic absorption ability. In summary, this work provides a valuable research idea for developing strong absorbing properties of absorbing materials at a low filling rate.

**Keywords:** Ni-MOF derivatives; polypyrrole; microwave absorption; polarization



**Citation:** Ma, Y.; Zou, Y.; Meng, L.; Cai, L.; Xiong, S.; Chen, G.; Dong, C.; Guan, H. Ni@C/PPy Composites Derived from Ni-MOF Materials for Efficient Microwave Absorption.

*Magnetochemistry* **2024**, *10*, 24.

<https://doi.org/10.3390/magnetochemistry10040024>

Academic Editor: Krzysztof Chwastek

Received: 1 March 2024

Revised: 22 March 2024

Accepted: 27 March 2024

Published: 30 March 2024



**Copyright:** © 2024 by the authors. Licensee MDPI, Basel, Switzerland. This article is an open access article distributed under the terms and conditions of the Creative Commons Attribution (CC BY) license (<https://creativecommons.org/licenses/by/4.0/>).

## 1. Introduction

The rapid development of modern communication technology has been stimulated and promoted to a large extent by the continuous emergence of various electronic devices. While these have greatly facilitated people's lives, they concurrently present an increasing number of electromagnetic pollution problems [1–5]. Therefore, to address the aforementioned issues, electromagnetic wave (EMW) absorbing materials have seen rapid development and extensive application across numerous sectors due to their ability to transform incoming electromagnetic waves into various forms of energy, thereby diminishing or dispersing the electromagnetic waves [6,7]. In recent decades, various kinds of EMW absorbing materials have emerged, such as magnetic dielectric absorbing materials (ultrafine metal powder and ferrite), dielectric absorbing materials (silicon nitride and iron nitride) and resistance-type absorbing materials (carbon black, silicon carbide and high conductivity polymer) [8–13].

Generally speaking, the ideal EMW absorbing material should encompass the following key features: robust absorption capacity, wide absorption band, a thin matched thickness and lightweight attributes [14]. One-component electromagnetic material, however, as a result of the limitation of the electromagnetic loss mechanism and poor performance of impedance matching, often finds it difficult to achieve the ideal absorption

effect. Therefore, the creation of and research into composite materials featuring multiple loss properties have increasingly emerged as highly sought-after areas of study within the domain of electromagnetic absorbing materials [12,15]. Ni-MOF, as a representative type of metal–organic framework (MOF) material, has a structure primarily constructed through the mutual coordination between nickel ions and organic ligands. Due to their structural and high-porosity characteristics, Ni-MOF-derived materials exhibit excellent electrical and magnetic properties, as well as abundant defect structures and interface properties after calcination at specific temperatures. These advantages make the material conducive to impedance matching and can effectively enhance the electromagnetic loss performance [16–21]. For example, Liu et al. controlled electromagnetic parameters by changing the carbonation temperature to achieve optimal impedance matching. Under the condition of a 40 wt% filling rate, the electromagnetic absorption performance is successfully achieved in the best state, and its minimum reflection loss ( $RL_{\min}$ ) value reaches  $-51.8$  dB [16]. Yang et al. successfully synthesized a series of Ni-MOF hollow spheres with different surface structures by adjusting the hydrothermal reaction time. This result significantly broadens the effective absorption bandwidth of the material. At a filling rate of 50 wt%, the effective absorption bandwidth of the Ni-MOF hollow sphere material is as high as 6.8 GHz [17]. Yan et al. successfully employed various types of organic ligands to synthesize two novel microsphere materials derived from Ni-MOF, namely Ni@C. When the filling rate of the Ni@C-ZIF sample is 40 wt%, the optimal  $RL_{\min}$  value of  $-86.8$  dB can be reached [21].

These results show that Ni-MOF magnetic carbon composites have considerable application prospects and excellent performance potential in the microwave absorption field. However, it usually has a high filling amount, which, to a certain extent, does not fully meet the “thin, light, broadband, efficient” performance standards. Therefore, multi-component or complex structures are usually used for optimization. For example, Xiang et al. constructed a 2D MXene-coated Ni@C lamellar composite with a nano/micron structure with a filling ratio of 8 wt%, which showed an excellent loss performance [22]. Xu et al. used a simple hydrothermal method and pyrolysis technology to successfully prepare a unique layered composite structure CoNi@NC material. Due to its distinctive construction properties, the composite not only exhibits excellent wave absorption properties at a filling rate of 20 wt% but also performs particularly well in broadening the absorption bandwidth [23]. Therefore, the combination of Ni-MOF-based magnetic carbon composite and dielectric material can effectively strengthen and optimize the synergistic effect between the multi-component composites, so as to provide the composite with excellent absorption properties under the condition of a lower filling ratio.

MXene, carbon and conductive polymer matrix composites are all dielectric materials with strong dielectric loss, and they have strong ability to absorb electromagnetic waves [15,22]. Among them, conductive polypyrrole (PPy) has been widely explored in EMW absorbing materials because of its advantages of light weight, high dielectric and easy synthesis. For example, the results of  $ZnFe_2O_4/C@PPy$  [24] and  $Al_2O_3@PPy@rGO$  [25] show that the introduction of PPy means that the composite material makes steady progress on the road to reducing the filling rate and thickness, and even at a very low filling rate and extremely thin thickness, it can still maintain its excellent electromagnetic absorption performance, thus opening up new possibilities for material design. Based on this, by integrating Ni@C with PPy, it is able to achieve significantly enhanced dielectric loss performance, while maintaining the original properties, and effectively combine the advantages of both components to improve synergistic effects among various loss mechanisms, so it is expected to obtain an EMW absorbing material with excellent performance.

In this paper, the Ni@C/PPy composite of Ni-MOF-derived nanoporous Ni@C-decorated tubular PPy was successfully fabricated using a self-assembly method. The interconnected tubular polypyrrole structure can provide abundant loading space for Ni@C nanoparticles due to its very high specific surface area while maintaining the enhanced effect of multiple reflections and refraction. Ni@C's special core–shell shape and surface defects can enhance

the loss capacity of Ni@C/PPy composites and optimize impedance matching. Therefore, the Ni@C/PPy composite has excellent absorption properties, with its  $RL_{\min}$  being  $-50.65$  dB, corresponding to a 6.24 GHz bandwidth. In summary, the present research results strongly reveal the excellent properties and broad application prospects of Ni@C/PPy composites, highlighting their great potential as electromagnetic absorbing materials.

## 2. Materials and Methods

### 2.1. Materials

Divinylbenzidine (Py), 4,4'-Biphenyldicarboxylic acid ( $H_2BPDC$ ), triethylene diamine ( $C_6H_{12}N_2$ ), methyl orange ( $C_{14}H_{14}N_3SO_3Na$ ), polyvinyl pyrrolidone (PVP), N,N-Dimethylformamide (DMF), ethyl alcohol ( $C_2H_6O$ ) and concentrated hydrochloric acid (HCl), Nickelous nitrate hexahydrate ( $Ni(NO_3)_2 \cdot 6H_2O$ ) and iron (3+) trichloride ( $FeCl_3 \cdot 6H_2O$ ) were obtained from Macklin Biochemical Co., Ltd. (Shanghai, China).

### 2.2. Preparation of Tubular PPy

Firstly, 6.75 g of  $FeCl_3 \cdot 6H_2O$  was added to 20 mL of deionized water, and solution A was obtained after complete dissolution. In addition, 0.15 g methyl orange was added to 30 mL deionized water and stirred vigorously for 10 min, and then 690  $\mu$ L pyrrole was added to the solution, and thus, solution B was obtained after continued stirring for 20 min. Immediately after that, we slowly poured Solution A into Solution B under room temperature conditions, followed by magnetic stirring until a uniform mixture was achieved, and then allowed it to stand for 24 h. Then, we filtered the mixture using suction filtration with 0.2 M hydrochloric acid and ethanol and finally washed the precipitation with deionized water until it was neutral. After drying at 60 °C, a black solid powder was obtained.

### 2.3. Preparation of Ni@C Composite Materials

Firstly, 40 mL DMF was mixed with 20 mL deionized water, then 0.58 g  $Ni(NO_3)_2 \cdot 6H_2O$  and 0.48 g 4,4'-biphenyl dicarboxylic acid ( $H_2BPDC$ ) were added to the mixed solution. This mixed solution was subsequently maintained at 130 °C for 24 h after the addition of 0.12 g  $C_6H_{12}N_2$ , followed by sonication for 30 min. After cooling, the precipitation was collected via centrifugation at 8000 rpm for 5 min and then washed 3 times each with DMF and ethanol. The resulting powder was dried at 70 °C for 12 h. Finally, the green powder was pyrolyzed at 500 °C in an Ar atmosphere and kept for 2 h to obtain the black Ni@C composite powder.

### 2.4. Preparation of Ni@C/PPy Composites

Firstly, 0.01 g of PPy powder was uniformly dispersed and dissolved in a 50 mL anhydrous ethanol solution with continuous stirring for 30 min to ensure thorough mixing. Subsequently, 0.03 g of Ni@C powder was added at a slow and steady rate, followed by re-stirring and dispersion treatment, after which the mixture underwent ultrasonic processing for 4 h to form a homogeneous solution. Upon the completion of these steps, the resulting precipitate was collected and subjected to constant temperature drying at 70 °C for 24 h, thereby preparing the composite material. To study the effect of PPy content on the absorption properties of materials, a series of Ni@C/PPy-x (x = 1, 2, 3, 4) composites with different polypyrrole contents (0.010 g, 0.015 g, 0.020 g, 0.025 g) was prepared.

### 2.5. Characterization

The characterization of the synthesized Ni@C and Ni@C/PPy composite materials was conducted using scanning electron microscopy (SEM, FEI Nova Nano SEM 450, Hillsboro, OR, USA), transmission electron microscopy (TEM, JEOL JEM-2100, Tokyo, Japan), a Fourier-transform infrared spectrometer (FT-IR, Thermofisher Bruck Nicolet iS 10, Waltham, MA, USA), Raman spectroscopy (Renishaw, London, UK), and X-ray diffraction (XRD, TTRIII, Tokyo, Japan). The electromagnetic parameters were tested within the radar

frequency range (2–18 GHz) using a vector network analyzer (VNA, Keysight P5004A, Santa Rosa, CA, USA). To do so, 15 wt% of Ni@C/PPy powder was uniformly mixed into an 85 wt% paraffin wax matrix, which was then carefully pressed into standard annular samples with inner diameters of 3.04 mm, outer diameters of 7.00 mm, and thicknesses of 2.00 mm. Before testing, the vector network analyzer was calibrated carefully using a Keysight electronic calibration module (ECal module N7554A) [26]. Subsequently, the electromagnetic parameters of these samples, including the complex permittivity ( $\epsilon_r$ ) and complex permeability ( $\mu_r$ ), were meticulously measured from the S parameters (S11, S21) via the Nicolson–Ross–Weir (NRW) method [27] using a coaxial air-line working in the frequency range of 2–18 GHz. Figure S1 in the Supporting Information shows the details of the calibration and testing process.

### 3. Results and Discussion

#### 3.1. Structural and Component Analysis

Figure 1 depicts the preparation process of the Ni@C/PPy composite. Firstly, Ni-MOF precursors and tubular PPy were obtained via simple hydrothermal and polymerization processes, respectively. Secondly, Ni@C was obtained via high-temperature calcination. Finally, the Ni@C/PPy composite material was successfully prepared by combining Ni@C and PPy through simple self-assembly.

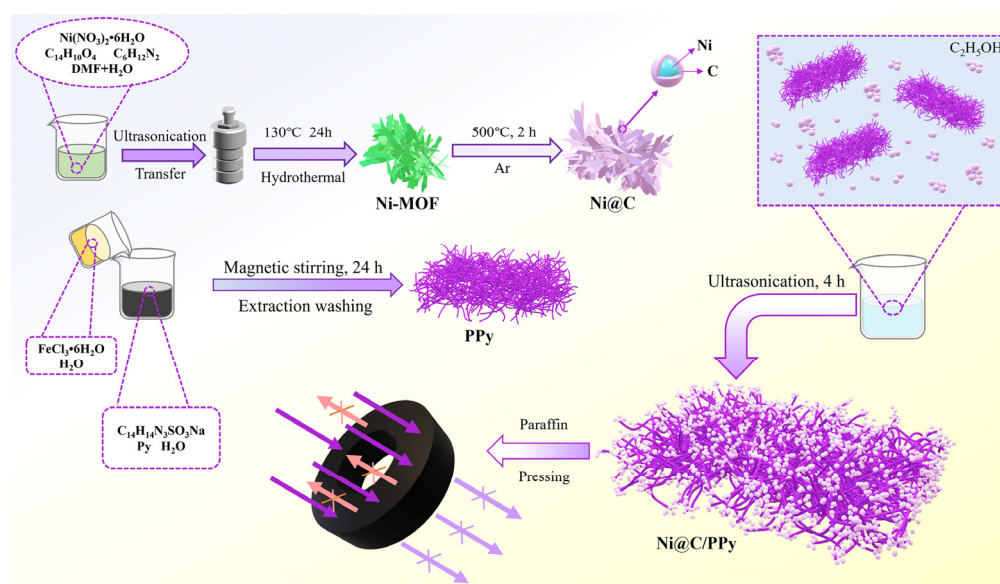


**Figure 1.** The preparation process of Ni@C/PPy composites.

The crystal structures of PPy, Ni@C and different proportions of Ni@C/PPy-x samples were investigated via XRD, with the results being shown in Figure 2a,b. Among them, PPy only has a wide peak centered at  $26.6^\circ$ , and there are no other diffraction peaks. However, in the two composites, Ni@C and Ni@C/PPy, three significant diffraction peaks were observed at approximately  $44.6^\circ$ ,  $51.9^\circ$  and  $76.5^\circ$ . These diffraction peaks correspond specifically to the (1 1 1), (2 0 0) and (2 2 0) crystal facet structures of face-centered cubic nickel (JCPDS no. 70-0989). There is a bulge of weak diffraction peaks belonging to PPy in the range of  $20^\circ$ – $30^\circ$  (Figure 2b). In the XRD analysis of the Ni@C/PPy composite, the characteristic peaks of PPy fail to appear because the characteristic peaks of Ni elements are too significant. We verified the successful preparation of Ni@C/PPy composites by using FTIR spectra. As shown in Figure 2c, the FTIR clearly revealed the presence of PPy components, thus confirming the success of the composite preparation. Compared with Ni@C, the Ni@C/PPy composite shows a unique characteristic peak because of its PPy component. The peak at  $1641\text{ cm}^{-1}$  corresponds to the C=C bond stretching vibration in the PPy ring, while the peak related to the stretching vibration of the C-C bond is located

near  $1170\text{ cm}^{-1}$ . The typical peaks induced by symmetric and asymmetric vibrations of the pyrrole ring are mainly concentrated in the two adjacent regions of  $1540\text{ cm}^{-1}$  and  $1450\text{ cm}^{-1}$ . The diffraction peak observed at  $1291\text{ cm}^{-1}$  is associated with the stretching mode of the C-N bond, and the peaks occurring at  $1024\text{ cm}^{-1}$  and  $904\text{ cm}^{-1}$  are indicative of the in-plane stretching vibrations of the N-H bonds within the molecular plane and the out-of-plane bending vibrations of the C-H bonds, respectively [24,28–31].

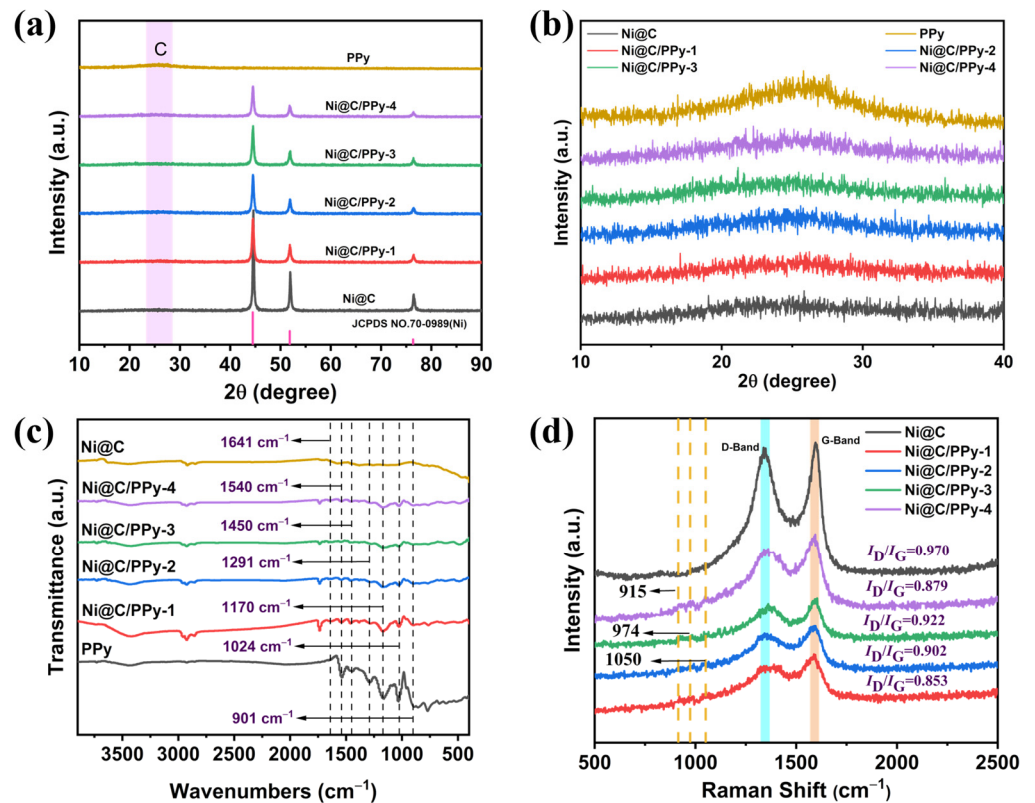


**Figure 2.** The XRD (a), locally amplified XRD (b) and FT-IR (c) images of the Ni@C, PPy and Ni@C/PPy composites. (d) Raman diagrams of Ni@C/PPy and Ni@C composites.

Raman characterization of the samples was performed to further explore the chemical compositions of the Ni@C/PPy composites, as shown in Figure 2d. Peaks with unique properties of PPy appeared in Ni@C/PPy composites, which strongly confirmed that the binding process of Ni@C and PPy was successful, and the chemical structure of PPy was effectively preserved during the binding process. The peak value at the position of  $1050\text{ cm}^{-1}$  can be interpreted as the deformation and vibration characteristics of the in-plane C-H bond. Meanwhile, the double peaks close to  $915\text{ cm}^{-1}$  and  $974\text{ cm}^{-1}$  are associated with the quinone polaron and bipolarized substructure [32]. In all the samples, two distinct Raman characteristic peaks can be obviously observed near  $1340\text{ cm}^{-1}$  and  $1590\text{ cm}^{-1}$ , corresponding to the D and G peaks, respectively. Since Ni@C composite is a magnetic carbon-based material, and its D-peak characteristics are usually derived from the defects in the amorphous carbon structure or graphite layer. The G band corresponds to the ordered graphite layer structure. In addition, the  $\pi$ -conjugated structure on the PPy backbone and ring stretching contribute to this outcome [33]. After the addition of PPy, the D and G peaks of the Ni@C/PPy composite were reduced, but the position was unchanged, which was due to the lower content of Ni@C in the composite. At the same time, it was found that among the four samples, Ni@C/PPy-3 had the largest  $I_D/I_G$  value, indicating that Ni@C/PPy-3 had more defects and greater disorder. This facilitates the production of higher dielectric losses, thereby improving the electromagnetic attenuation of the composites.

### 3.2. Morphological Analysis

The microscopic morphologies of Ni-MOF, Ni@C, PPy and Ni@C/PPy composites are characterized. As shown in Figure 3a and Figure S2, Ni-MOF shows a regular sheet-like structure similar to bamboo leaves, and the Ni@C composite obtained after high-temperature pyrolysis shows a rough outline of the precursor Ni-MOF, and its surface is relatively rough, as in Figure 3b. In addition, Ni@C composites are cleverly constructed from countless closely connected Ni@C spheres, forming an ordered and continuous structural layout (Figures 3e and S3). HRTEM pictures further show that Ni, as a spherical center, is tightly wrapped by the carbon layer, and the lattice stripes of carbon and the corresponding face-centered cubic nickel (1 1 1) are clearly visible (Figure 3h). However, PPy shows a 3D network morphology formed by the mutual cross-linking of one-dimensional tubular structures (Figure 3c), which not only helps Ni@C nanoparticles to better adsorb on the surface but also significantly increases the transmission path length of the incident electromagnetic wave, thereby increasing the number of electromagnetic wave reflections. The one-dimensional tubular structure of PPy can also be further seen through HRTEM images in Figure 3f. The Ni/C nanoparticles are more uniformly adsorbed outside PPy agglomeration, forming cross-linked PPy tubes inside and scattered Ni@C particles outside (Figure 3d,g,i). This complex multidimensional structure can enhance the interface polarization and, thus, bring about an increase in conduction loss. Figure S4 shows the SEM images of the annular sample prepared by mixing 15 wt% Ni@C/PPy powder and 85 wt% paraffin wax. It can be clearly seen that Ni@C/PPy powder and paraffin wax are evenly mixed.

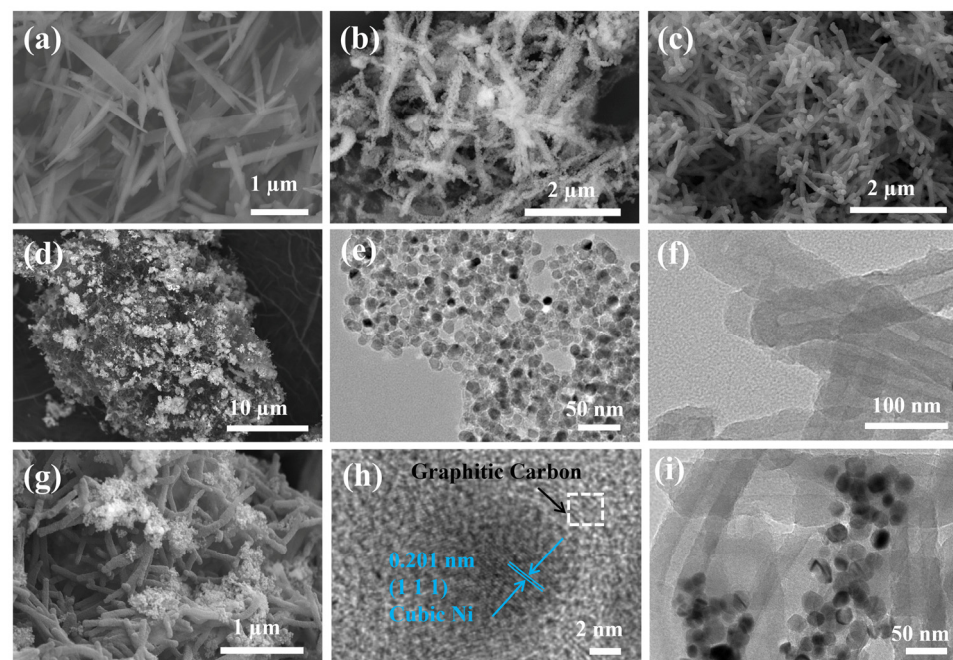


**Figure 3.** SEM images of Ni-MOF (a), Ni@C (b), PPy (c) and Ni@C/PPy-3 (d,g). TEM images of Ni@C (e,h) and Ni@C/PPy-3 (f,i).

### 3.3. Electromagnetic Characterization

In general, the accurate evaluation of electromagnetic wave absorption performance depends heavily on the electromagnetic parameters of the absorber, which include the complex dielectric constant ( $\epsilon_r = \epsilon' - j\epsilon''$ ) and the magnetic permeability ( $\mu_r = \mu' - j\mu''$ ). The real parts of the dielectric constant ( $\epsilon'$ ) and permeability ( $\mu'$ ) mainly reflect the ability of the material to store electrical energy and magnetic energy. Their imaginary parts,  $\epsilon''$  and  $\mu''$ , stand for the extent to which the material loses or dissipates electrical and magnetic energy under electromagnetic action, respectively. In addition, the frequency-dependent

electromagnetic parameters and reflection loss performance for pure paraffin are shown in Figure S5. As can be observed in Figure S5, paraffin has much lower dielectric permittivity and magnetic permeability, which leads to the result that paraffin is almost transparent to microwaves. It means that the main difference in the electromagnetic parameter values of the samples is mainly due to the conductivity characteristics of the sample itself [7].

The electromagnetic parameters of Ni@C and Ni@C/PPy-*x* composites are shown in Figure 4. The  $\epsilon'$  and  $\epsilon''$  values of pure Ni@C material are relatively low, which indicates that pure Ni@C material has poor interaction with electromagnetic waves (Figure 4a,b). In the category of composite materials, the addition of PPy can significantly increase its dielectric constant, and this value will continue to increase with the gradual increase in the PPy dosage. This reveals the dual advantages brought about by the doping of PPy as a conductive polymer. On one hand, it facilitates the construction of internal conductive networks; on the other hand, it provides more adhesion interfaces for Ni@C particles, thus reducing the agglomeration phenomenon between Ni@C particles. At the same time, it is more conducive to the tight combination between PPy and Ni@C. Therefore, in this way, the dielectric constant of the composite can be effectively regulated, thus improving its ability to store incident EMW.

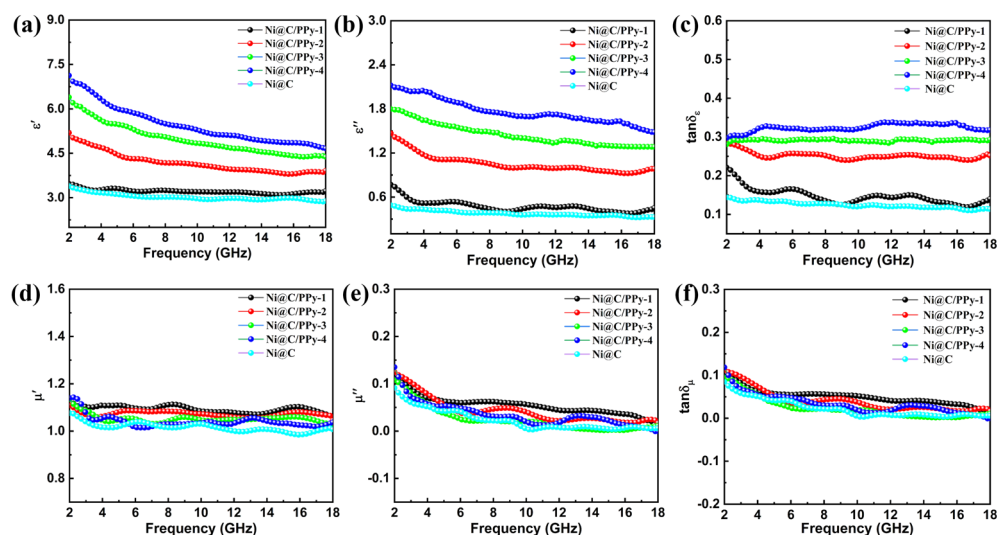


**Figure 4.** The complex permittivity (a,b), permeability (d,e), dielectric loss (c) and magnetic loss (f) of the Ni@C and Ni@C/PPy composites.

In the whole frequency band,  $\epsilon'$  and  $\epsilon''$  of pure Ni@C fluctuated between 3.59 and 3.08 and 0.48 and 0.32, respectively. In contrast,  $\epsilon'$  of Ni@C/PPy-*x* decreased from 3.46 to 3.22, 5.19 to 3.91, 6.39 to 4.37 and 7.12 to 4.66, respectively. At the same time, the  $\epsilon''$  varies from 0.76 to 0.45, 1.46 to 0.98, 1.79 to 1.28 and 2.11 to 1.48, respectively. Moreover, the values of all samples decreased throughout the testing frequency range, which is due to the dispersive behavior of the frequency. This is also related to the phenomenon of electromagnetic energy dissipation, which is caused by the oriented polarization of the dipole [34]. Therefore, the decrease in the complex dielectric permittivity is due to the fact that the electron cannot adapt to the rapid shortening of the period of the high-frequency alternating electromagnetic field [28].

The parameter  $\tan\delta_\epsilon$  can be used to evaluate the dielectric loss properties of Ni@C/PPy composites and Ni@C materials. The higher the  $\tan\delta_\epsilon$  value, the better the material absorbs electromagnetic waves [35,36]. The trend of  $\tan\delta_\epsilon$  values is consistent with the trend of  $\epsilon''$  (Figure 4c). Pure Ni@C has a lower  $\tan\delta_\epsilon$  value, while the Ni@C/PPy composite exhibits a higher  $\tan\delta_\epsilon$  value. This phenomenon is mainly attributed to the existence of the PPy component, which strongly proves that PPy has better dielectric loss performance. For permeability, the values of the  $\mu'$  and  $\mu''$  parameters fluctuated around 1 and 0 for all samples, respectively, indicating that the effect of magnetic losses is small, as in Figure 4d,e.

The curve of the tangent value of magnetic loss ( $\tan\delta_\mu = \mu''/\mu'$ ) in Figure 4f is basically consistent with the curve of  $\mu''$  and is much smaller than  $\tan\delta_\epsilon$ , which further indicates that the primary microwave attenuation mechanism in these samples is predominantly attributed to dielectric loss.

Using the transmission line theory, the electromagnetic absorption properties of Ni@C/PPy composites, termed reflection loss (RL), can be accurately calculated. The three-dimensional RL diagram of Ni@C and Ni@C/PPy composites within the frequency range of 2–18 GHz can be derived using Formulas (1) and (2) [37] as follows:

$$RL(\text{dB}) = 20\log_{10} \left| \frac{Z_{in} - Z_0}{Z_{in} + Z_0} \right| \quad (1)$$

$$Z_{in} = Z_0 \sqrt{\mu_r/\epsilon_r} \tanh[j(2\pi fd/c) \sqrt{\mu_r\epsilon_r}] \quad (2)$$

In the formulas,  $Z_{in}$  and  $Z_0$  are the input impedance and the impedance of free space, respectively. In addition,  $c$  is set to the speed of light in vacuum, i.e., the value of  $3 \times 10^8$  m/s. At the same time,  $d$  and  $f$  denote the thickness of the material and the frequency of the electromagnetic wave passed, respectively. Typically, when the absorption and attenuation of electromagnetic energy by the material exceeds 90%, the RL value is below  $-10$  dB, the lower the RL value, the better the absorption performance of the material. And the associated frequency range ( $RL < -10$  dB) is defined as the effective absorption bandwidth (EAB).

Figure 5 illustrates the 3D RL and 2D bandwidth diagrams for all samples in the test frequency range. When the filling rate is 15 wt %, pure Ni @ C due to its low dielectric properties, the insufficient  $RL_{\min}$   $-10$  dB (Figure 5a,b), which cannot effectively absorb and attenuate electromagnetic waves. The introduction of the PPy tube results in a notable enhancement of electromagnetic wave absorption performance due to the increased dielectric loss and conduction loss. For Ni@C/PPy-1, the performance is not ideal, with  $RL_{\min}$  only slightly below  $-10$  dB (Figure 5c,d). Figure 5e,f show the absorption performance of Ni@C/PPy-2. Compared with Ni@C/PPy-1, Ni@C/PPy-2 shows a stronger absorption performance, with its  $RL_{\min}$  value reaching  $-25.96$  dB. The best performance is achieved with Ni@C/PPy-3 composite, with an EAB of 6.24 GHz and a  $RL_{\min}$  of  $-50.65$  dB at the thickness of 2.5 mm, as in Figure 5g,h. Nevertheless, with the continuous increase in PPy content, the composite material experienced impedance mismatching, causing its wave absorption performance to begin to decrease. The performance of Ni@C/PPy-4 is not as good as that of Ni@C/PPy-3, and its absorption performance is reduced, as in Figure 5i,j. In addition, comparing the RL values of Ni@C/PPy composites at the filling rates of 10 wt%, 15 wt% and 20 wt% (Figure S6), it is still found that Ni@C/PPy-3 at the filling rate of 15 wt% has the best microwave absorption performance. In Figure 5k, both the  $RL_{\min}$  and EAB values for all samples can be clearly observed. Clearly, the Ni@C/PPy-3 sample demonstrated the best microwave absorption performance, which was mainly due to the introduction of the conductive polymer PPy. Ni@C particles attach to the outer surface of the tubular aggregate PPy, creating a complex structure of interwoven tubes inside and Ni@C particles outside. By enhancing the reflection and scattering times of the microwave on the surface and inside, the propagation path of the incident microwave can be effectively prolonged and its energy dissipation efficiency can be improved. In addition, by determining the best dosage of PPy, the synergistic effect between PPy and Ni@C can be effectively strengthened, the impedance matching can be optimized, and, finally, the excellent performance of absorbing materials can be prepared.

Whether the absorbing material has good absorbing performance is largely related to impedance matching ( $Z = |Z_{in}/Z_0|$ ). Under normal circumstances, the key condition for the effective entry of electromagnetic waves into the material is to achieve an ideal impedance matching state, that is,  $Z$  equals 1. When the impedance matching coefficient of the material is in the range of 0.8 to 1.2, the closer it is to 1, the better the impedance matching performance [38]. It can be clearly seen that the Ni@C/PPy composite material occupies

a larger area in the range of 0.8–1.2 compared with pure Ni@C material (Figure 6a–e). Through the introduction of PPy material, the conductivity of the composite is successfully regulated, and the impedance matching performance is significantly improved. This improvement significantly reduces the reflection of electromagnetic waves on the surface of the material, so that most electromagnetic waves can effectively penetrate and transmit deep into the material [39]. In the Ni@C/PPy composites, Ni@C/PPy-3 has a larger and more concentrated impedance area than the other samples. The above results show that the Ni@C/PPy-3 composite has the best impedance matching, which gives Ni@C/PPy-3 excellent microwave absorption capacity. This is consistent with the obtained RL results. Simultaneously, this shows that the right amount of PPy will optimize the impedance matching and, thus, improve its absorption performance.

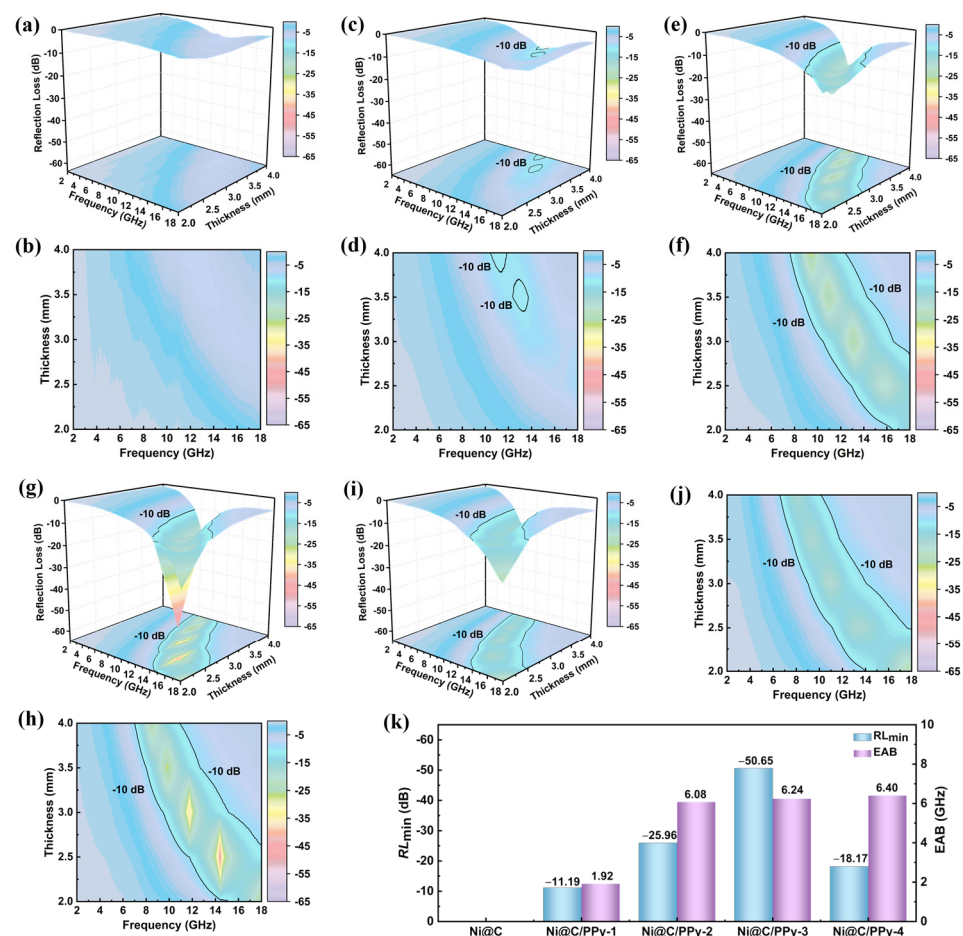


**Figure 5.** Three-dimensional RL (a–j) and absorption bandwidth (k) diagrams of Ni@C (a,b), Ni@C/PPy-1 (c,d), Ni@C/PPy-2 (e,f), Ni@C/PPy-3 (g,h) and Ni@C/PPy-4 (i,j).

In order to deeply investigate the dielectric loss characteristics of the sample, the internal relationship between the Cole–Cole semicircle model and the relaxation phenomenon is successfully constructed by using the Debye relaxation theory. The specific expression of this connection can be precisely elaborated based on the relationship between  $\epsilon'$  and  $\epsilon''$  [40]:

$$\left(\epsilon' - \frac{\epsilon_s + \epsilon_\infty}{2}\right)^2 + (\epsilon'')^2 = \left(\frac{\epsilon_s - \epsilon_\infty}{2}\right)^2 \quad (3)$$

where  $\epsilon_s$  represents the static dielectric constant, while  $\epsilon_\infty$  and  $\tau$  denote the high-frequency effective dielectric constant and relaxation time, respectively. The semicircles observed in the  $\epsilon''$ - $\epsilon'$  curves are referred as Cole–Cole semicircles. Each presence of an independent Debye relaxation process is presented as a semicircle, while the presence of conduction

losses results in a straight line at the tail of the curve. As shown in Figure S7a–e, multiple Debye relaxation processes are evident in Ni@C and Ni@C/PPy-x. However, Ni@C/PPy composites exhibit more irregular Debye semicircle structures than pure Ni@C. This means that Ni@C/PPy composites have more significant dielectric polarization relaxation properties. These properties may be due to the presence of PPy inside the sample, which promotes an increase in the number of polarized charges and the enhancement of the interface effect, thus triggering a greater dielectric relaxation loss [41]. Therefore, the Ni@C/PPy composite exhibits excellent electromagnetic wave absorption properties.

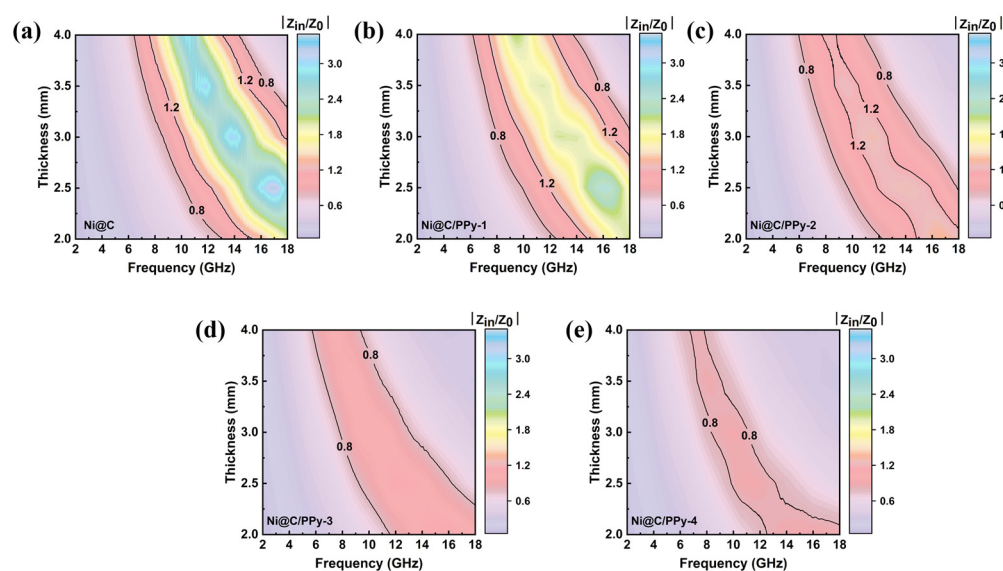


**Figure 6.** Impedance matching plots of the samples Ni@C (a), Ni@C/PPy-1 (b), Ni@C/PPy-2 (c), Ni@C/PPy-3 (d) and Ni@C/PPy-4 (e).

#### 4. Conclusions

This study employed a straightforward self-assembly method to fabricate Ni@C/PPy composites. By adjusting the PPy content, the dielectric parameters of the composites were efficiently optimized, resulting in the successful attainment of a Ni@C/PPy composite exhibiting superior microwave absorption performance. Ni@C/PPy-3 demonstrates the most outstanding microwave absorption performance, achieving a peak  $RL_{\min}$  value of  $-50.65$  dB. The corresponding EAB is up to 6.24 GHz (11.76–18 GHz) under an optimal thickness of 2.5 mm. The findings indicate that the Ni@C/PPy composite possesses highly desirable characteristics as an electromagnetic absorbent material. These include effective dielectric loss, magnetic loss and synergistic electromagnetic coordination, complemented by the multiple reflection effects facilitated by the combined features of Ni@C and PPy tubes.

**Supplementary Materials:** The following supporting information can be downloaded at: <https://www.mdpi.com/article/10.3390/magnetochemistry10040024/s1>, Figure S1: The calibration and testing process; Figure S2: SEM diagram of the Ni-MOF particles; Figure S3: TEM view of the Ni@C composite; Figure S4: SEM of the annular samples mixed with Ni@C/PPy powder and paraffin matrix at a 15 wt% filling ratio; Figure S5: Electromagnetic parameters and reflection loss plots versus frequency for pure paraffin; Figure S6: The reflection loss of Ni@C/PPy-1, Ni@C/PPy-2, Ni@C/PPy-3 and Ni@C/PPy-4 with a filling ratio of 10 wt%, 15 wt% and 20 wt%; Figure S7: The Cole–Cole curves of Ni@C, Ni@C/PPy-1, Ni@C/PPy-2, Ni@C/PPy-3 and Ni@C/PPy-4.

**Author Contributions:** Conceptualization, Y.M. and H.G.; methodology, Y.M. and L.M.; validation, G.C.; investigation, Y.M., Y.Z. and L.C.; data curation, Y.M. and S.X.; writing—original draft preparation, Y.M.; writing—review and editing, H.G. and C.D.; supervision, H.G.; funding acquisition, G.C. and H.G. All authors have read and agreed to the published version of the manuscript.

**Funding:** This study was funded by the Natural Science Foundation of China (NSFC, grant no. 22165032), the Major Science and Technology Special Fund of Yunnan Province (grant no. 202102AB080019-3) and Yunnan University's Practice Innovation Project for Professional Degree Graduate Students (grant no. ZC-22222859).

**Institutional Review Board Statement:** Not applicable.

**Informed Consent Statement:** Not applicable.

**Data Availability Statement:** The data presented in this study are available on request from the corresponding author.

**Acknowledgments:** The authors thank the Advanced Analysis and Measurement Center of Yunnan University for providing the sample testing service.

**Conflicts of Interest:** The authors declare no conflicts of interest.

## References

1. Ma, L.; Hamidinejad, M.; Liang, C.; Zhao, B.; Habibpour, S.; Yu, A.; Filleter, T.; Park, C.B. Enhanced electromagnetic wave absorption performance of polymer/SiC-nanowire/MXene ( $\text{Ti}_3\text{C}_2\text{T}_x$ ) composites. *Carbon* **2021**, *179*, 408–416. [[CrossRef](#)]
2. Zhang, S.; Jia, Z.; Cheng, B.; Zhao, Z.; Lu, F.; Wu, G. Recent progress of perovskite oxides and their hybrids for electromagnetic wave absorption: A mini-review. *Adv. Compos. Hybrid Mater.* **2022**, *5*, 2440–2460. [[CrossRef](#)]
3. Xu, J.; Cao, J.; Guo, M.; Yang, S.; Yao, H.; Lei, M.; Hao, Y.; Bi, K. Metamaterial mechanical antenna for very low frequency wireless communication. *Adv. Compos. Hybrid Mater.* **2021**, *4*, 761–767. [[CrossRef](#)]
4. Ruan, J.; Chang, Z.; Rong, H.; Alomar, T.S.; Zhu, D.; AlMasoud, N.; Liao, Y.; Zhao, R.; Zhao, X.; Li, Y.; et al. High-conductivity nickel shells encapsulated wood-derived porous carbon for improved electromagnetic interference shielding. *Carbon* **2023**, *213*, 118208. [[CrossRef](#)]
5. Guo, J.; Chen, Z.; Xu, X.; Li, X.; Liu, H.; Xi, S.; Abdul, W.; Wu, Q.; Zhang, P.; Bin Xu, B.; et al. Enhanced electromagnetic wave absorption of engineered epoxy nanocomposites with the assistance of polyaniline fillers. *Adv. Compos. Hybrid Mater.* **2022**, *5*, 1769–1777. [[CrossRef](#)]
6. Zhang, S.; Cheng, B.; Jia, Z.; Zhao, Z.; Jin, X.; Zhao, Z.; Wu, G. The art of framework construction: Hollow-structured materials toward high-efficiency electromagnetic wave absorption. *Adv. Compos. Hybrid Mater.* **2022**, *5*, 1658–1698. [[CrossRef](#)]
7. Chang, Q.; Liang, H.; Shi, B.; Li, X.; Zhang, Y.; Zhang, L.; Wu, H. Ethylenediamine-assisted hydrothermal synthesis of  $\text{NiCo}_2\text{O}_4$  absorber with controlled morphology and excellent absorbing performance. *J. Colloid Interface Sci.* **2021**, *588*, 336–345. [[CrossRef](#)] [[PubMed](#)]
8. Liang, C.; Qiu, H.; Song, P.; Shi, X.; Kong, J.; Gu, J. Ultra-light MXene aerogel/wood-derived porous carbon composites with wall-like “mortar/brick” structures for electromagnetic interference shielding. *Sci. Bull.* **2020**, *65*, 616–622. [[CrossRef](#)] [[PubMed](#)]
9. Zhang, S.; Cheng, B.; Gao, Z.; Lan, D.; Zhao, Z.; Wei, F.; Zhu, Q.; Lu, X.; Wu, G. Two-dimensional nanomaterials for high-efficiency electromagnetic wave absorption: An overview of recent advances and prospects. *J. Alloys Compd.* **2022**, *893*, 162343. [[CrossRef](#)]
10. Gao, Z.; Lan, D.; Zhang, L.; Wu, H. Simultaneous manipulation of interfacial and defects polarization toward Zn/Co phase and ion hybrids for electromagnetic wave absorption. *Adv. Funct. Mater.* **2021**, *31*, 2106677. [[CrossRef](#)]
11. Liu, J.; Che, R.; Chen, H.; Zhang, F.; Xia, F.; Wu, Q.; Wang, M. Microwave absorption enhancement of multifunctional composite microspheres with spinel  $\text{Fe}_3\text{O}_4$  cores and anatase  $\text{TiO}_2$  shells. *Small* **2012**, *8*, 1214–1221. [[CrossRef](#)] [[PubMed](#)]
12. Song, Q.; Ye, F.; Kong, L.; Shen, Q.; Han, L.; Feng, L.; Yu, G.; Pan, Y.; Li, H. Graphene and MXene nanomaterials: Toward high-performance electromagnetic wave absorption in gigahertz band range. *Adv. Funct. Mater.* **2020**, *30*, 2000475. [[CrossRef](#)]
13. Lan, D.; Gao, Z.; Zhao, Z.; Kou, K.; Wu, H. Application progress of conductive conjugated polymers in electromagnetic wave absorbing composites. *Compos. Commun.* **2021**, *26*, 100767. [[CrossRef](#)]
14. Zhou, X.; Jia, Z.; Feng, A.; Qu, S.; Wang, X.; Liu, X.; Wang, B.; Wu, G. Synthesis of porous carbon embedded with  $\text{NiCo}/\text{CoNiO}_2$  hybrids composites for excellent electromagnetic wave absorption performance. *J. Colloid Interface Sci.* **2020**, *575*, 130–139. [[CrossRef](#)] [[PubMed](#)]
15. Wu, G.; Jia, Z.; Zhou, X.; Nie, G.; Lv, H. Interlayer controllable of hierarchical MWCNTs@C@FexOy cross-linked composite with wideband electromagnetic absorption performance. *Compos. Part A Appl. Sci. Manuf.* **2020**, *128*, 105687. [[CrossRef](#)]
16. Liu, W.; Shao, Q.; Ji, G.; Liang, X.; Cheng, Y.; Quan, B.; Du, Y. Metal-organic-frameworks derived porous carbon-wrapped Ni composites with optimized impedance matching as excellent lightweight electromagnetic wave absorber. *Chem. Eng. J.* **2017**, *313*, 734–744. [[CrossRef](#)]
17. Yang, Z.; Zhang, Y.; Li, M.; Yang, L.; Liu, J.; Hou, Y.; Yang, Y. Surface architecture of Ni-based metal organic framework hollow spheres for adjustable microwave absorption. *ACS Appl. Nano Mater.* **2019**, *2*, 7888–7897. [[CrossRef](#)]
18. Zhang, Z.; Zhu, Q.; Chen, X.; Wu, Z.; He, Y.; Lv, Y.; Zhang, L.; Zou, Y. Ni@C composites derived from Ni-based metal organic frameworks with a lightweight, ultrathin, broadband and highly efficient microwave absorbing properties. *Appl. Phys. Express* **2019**, *12*, 011001. [[CrossRef](#)]

19. Zhao, X.; Bei, M.; Liu, F.; Bu, F.; Jiang, X.; Yu, L. Solvent-conditioned Ni-MOF-derived flower-like porous carbon composites for electromagnetic wave absorption. *Synth. Met.* **2023**, *293*, 117294. [[CrossRef](#)]
20. Xiang, Z.; Zhang, X.; Shi, Y.; Cai, L.; Cheng, J.; Jiang, H.; Zhu, X.; Dong, Y.; Lu, W. Efficient microwave absorption of MOFs derived laminated porous Ni@C nanocomposites with waterproof and infrared shielding versatility. *Carbon* **2021**, *185*, 477–490. [[CrossRef](#)]
21. Yan, J.; Huang, Y.; Yan, Y.; Ding, L.; Liu, P. High-performance electromagnetic wave absorbers based on two kinds of nickel-based MOF-derived Ni@C microspheres. *ACS Appl. Mater. Interfaces* **2019**, *11*, 40781–40792. [[CrossRef](#)] [[PubMed](#)]
22. Xiang, Z.; Wang, X.; Zhang, X.; Shi, Y.; Cai, L.; Zhu, X.; Dong, Y.; Lu, W. Self-assembly of nano/microstructured 2D Ti<sub>3</sub>CNT<sub>x</sub> MXene-based composites for electromagnetic pollution elimination and Joule energy conversion application. *Carbon* **2022**, *189*, 305–318. [[CrossRef](#)]
23. Xu, X.; Ran, F.; Fan, Z.; Cheng, Z.; Lv, T.; Shao, L.; Liu, Y. Bimetallic metal–organic framework-derived pomegranate-like nanoclusters coupled with CoNi-doped graphene for strong wideband microwave absorption. *ACS Appl. Mater. Interfaces* **2020**, *12*, 17870–17880. [[CrossRef](#)] [[PubMed](#)]
24. Liao, Z.; Ma, M.; Tong, Z.; Wang, R.; Bi, Y.; Chen, Y.; Chung, K.L.; Ma, Y. Fabrication of ZnFe<sub>2</sub>O<sub>4</sub>/C@PPy composites with efficient electromagnetic wave absorption properties. *J. Colloid Interface Sci.* **2021**, *602*, 602–611. [[CrossRef](#)] [[PubMed](#)]
25. Lai, Y.; Lv, L.; Fu, H. Preparation and study of Al<sub>2</sub>O<sub>3</sub>@PPy@rGO composites with microwave absorption properties. *J. Alloys Compd.* **2020**, *832*, 152957. [[CrossRef](#)]
26. Rumiantsev, A.; Ridler, N. VNA calibration. *IEEE Microw. Mag.* **2008**, *9*, 86–99. [[CrossRef](#)]
27. Nicolson, A.M.; Ross, G.F. Measurement of the Intrinsic Properties of Materials by Time-Domain Techniques. *IEEE Trans. Instrum. Meas.* **1970**, *19*, 377–382. [[CrossRef](#)]
28. Gai, L.; Zhao, Y.; Song, G.; An, Q.; Xiao, Z.; Zhai, S.; Li, Z. Construction of core-shell PPy@MoS<sub>2</sub> with nanotube-like heterostructures for electromagnetic wave absorption: Assembly and enhanced mechanism. *Compos. Part A Appl. Sci. Manuf.* **2020**, *136*, 105965. [[CrossRef](#)]
29. Xie, A.; Sun, M.; Zhang, K.; Xia, Y.; Wu, F. Tetrazole amphiphile inducing growth of conducting polymers hierarchical nanostructures and their electromagnetic absorption properties. *Nanotechnology* **2018**, *29*, 215604. [[CrossRef](#)]
30. Xie, D.; Zhang, M.; Cheng, F.; Fan, H.; Xie, S.; Liu, P.; Tu, J. Hierarchical MoS<sub>2</sub>@Polypyrrole core-shell microspheres with enhanced electrochemical performances for lithium storage. *Electrochim. Acta* **2018**, *269*, 632–639. [[CrossRef](#)]
31. Chang, C.; Yang, X.; Xiang, S.; Que, H.; Li, M. Layered MoS<sub>2</sub>/PPy nanotube composites with enhanced performance for supercapacitors. *J. Mater. Sci. Mater. Electron.* **2016**, *28*, 1777–1784. [[CrossRef](#)]
32. Gu, H.; Huang, J.; Li, N.; Yang, H.; Wang, Y. Polystyrene-modulated polypyrrole to achieve controllable electromagnetic-wave absorption with enhanced environmental stability. *Nanomaterials* **2022**, *12*, 2698. [[CrossRef](#)] [[PubMed](#)]
33. Fan, X.; Yang, Z.; He, N. Hierarchical nanostructured polypyrrole/graphene composites as supercapacitor electrode. *RSC Adv.* **2015**, *5*, 15096–15102. [[CrossRef](#)]
34. Bi, Y.; Ma, M.; Liao, Z.; Tong, Z.; Chen, Y.; Wang, R.; Ma, Y.; Wu, G. One-dimensional Ni@Co/C@PPy composites for superior electromagnetic wave absorption. *J. Colloid Interface Sci.* **2022**, *605*, 483–492. [[CrossRef](#)] [[PubMed](#)]
35. Pan, D.; Yang, G.; Abo-Dief, H.M.; Dong, J.; Su, F.; Liu, C.; Li, Y.; Bin Xu, B.; Murugadoss, V.; Naik, N.; et al. Vertically aligned silicon carbide nanowires/boron nitride cellulose aerogel networks enhanced thermal conductivity and electromagnetic absorbing of epoxy composites. *Nano-Micro Lett.* **2022**, *14*, 118. [[CrossRef](#)] [[PubMed](#)]
36. Wang, L.; Wen, B.; Bai, X.; Liu, C.; Yang, H. NiCo alloy/carbon nanorods decorated with carbon nanotubes for microwave absorption. *ACS Appl. Nano Mater.* **2019**, *2*, 7827–7838. [[CrossRef](#)]
37. Huang, Z.; Ma, R.; Zhou, J.; Wang, L.; Xie, Q. Investigation on microstructures, electronic structures, electromagnetic properties and microwave absorption properties of Fe<sub>3</sub>Si/PPy composites. *J. Alloys Compd.* **2021**, *873*, 159779. [[CrossRef](#)]
38. Ren, H.; Li, T.; Wang, H.; Guo, Z.; Chen, T.; Meng, F. Two birds with one stone: Superhelical chiral polypyrrole towards high-performance electromagnetic wave absorption and corrosion protection. *Chem. Eng. J.* **2022**, *427*, 131582. [[CrossRef](#)]
39. Pan, F.; Rao, Y.; Batalu, D.; Cai, L.; Dong, Y.; Zhu, X.; Shi, Y.; Shi, Z.; Liu, Y.; Lu, W. Macroscopic electromagnetic cooperative network-enhanced MXene/Ni chains aerogel-based microwave absorber with ultra-low matching thickness. *Nano-Micro Lett.* **2022**, *14*, 140. [[CrossRef](#)]
40. Cole, K.S.; Cole, R.H. Dispersion and Absorption in Dielectrics I. Alternating Current Characteristics. *J. Chem. Phys.* **1941**, *9*, 341–351. [[CrossRef](#)]
41. Liu, S.; Fang, D.; Xing, F.; Jin, H.; Li, J. Auricularia-shaped MoS<sub>2</sub> nanosheet arrays coated hierarchical multilayer MoS<sub>2</sub>/PPy/rGO composites for efficient microwave absorption. *Chem. Eng. J.* **2024**, *479*, 147613. [[CrossRef](#)]

**Disclaimer/Publisher’s Note:** The statements, opinions and data contained in all publications are solely those of the individual author(s) and contributor(s) and not of MDPI and/or the editor(s). MDPI and/or the editor(s) disclaim responsibility for any injury to people or property resulting from any ideas, methods, instructions or products referred to in the content.